Condensin-Mediated Chromosome Folding and Internal Telomeres Drive Dicentric Severing by Cytokinesis

Thomas Guerin, Claire Béneut, Natalja Barinova, Virginia López, Luciana Lazar-Stefanita, Alice Deshayes, Agnès Thierry, Romain Koszul, Karine Dubrana, Stephane Marcand

HAL Id: pasteur-02866762
https://pasteur.hal.science/pasteur-02866762

Submitted on 25 Oct 2021

Condensin-mediated chromosome folding and internal telomeres drive dicentric severing by cytokinesis

Thomas M. GUÉRIN[1], Claire BÉNEUT[1], Natalja BARINOVA[1], Virginia LÓPEZ[1], Luciana LAZAR-STEFANITA[2], Alice DESHAYES[1], Agnès THIERRY[2], Romain KOSZUL[2], Karine DUBRANA[1] and Stéphane MARCAND[1,3]*

1. CEA Paris-Saclay, Unité Stabilité Génétique Cellules Souches et Radiations, INSERM U1274, Université de Paris, Université Paris-Saclay, France
2. Institut Pasteur, Unité Régulation Spatiale des Génomes, CNRS UMR 3525, Sorbonne Université, Paris, France
3. Lead contact

* Correspondence: stephane.marcand@cea.fr

Abstract

In *Saccharomyces cerevisiae*, dicentric chromosomes stemming from telomere fusions preferentially break at the fusion. This process restores a normal karyotype and protects chromosomes from the detrimental consequences of accidental fusions. Here we address the molecular basis of this rescue pathway. We observe that tandem arrays tightly bound by the telomere factor Rap1 or a heterologous high-affinity DNA binding factor are sufficient to establish breakage hotspots, mimicking telomere fusions within dicentrics. We also show that condensins generate forces sufficient to rapidly refold dicentrics prior to breakage by cytokinesis and are essential to the preferential breakage at telomere fusions. Thus, the rescue of fused telomeres results from a condensin- and Rap1-driven chromosome folding that favours fusion entrapment where abscission takes place. Since a close spacing between the DNA-bound Rap1 molecules is essential to this process, Rap1 may act by stalling condensins.

Introduction

Dicentric chromosomes, i.e. chromosomes with two active centromeres, are unstable structures that stem from erroneous DNA repair events or abnormal epigenetic neocentromere formation. When dicentrics are formed prior to replication, the two centromeres on the same sister chromatid are pulled towards either the same spindle pole or opposite poles with equal probability (Figure 1A). Migration to the same pole propagates the dicentric chromosome intact to the next generation whereas migration to opposite poles generates anaphase bridges, which often result in chromosome breakage (Hill and Bloom, 1989; McClintock, 1941; Thrower and Bloom, 2001). This breakage does not occur in anaphase but after mitotic spindle disassembly and the onset of cytokinesis (Hong et al., 2018a; Hou and Cooper, 2018; López et al., 2015; Maciejowski et al., 2015; Mohebi et al., 2015; Pampalona et al., 2016).

The newly broken ends can cause cell death or be subjected to DNA repair processes. Because they can enter into breakage-fusion-bridge cycles and lead to chromothripsis, dicentrics are a threat to cell viability and a source of extensive genome instability and mutagenesis (Beyer and Weinert, 2016; Maciejowski et al., 2015; McClintock, 1941). In normal contexts, dicentrics are rare. First, DNA repair is usually accurate enough to avoid chromosome translocations (Bétermier et al., 2014). Second, nonhomologous end-joining (NHEJ) is inhibited at telomeres, preventing telomere fusions that would generate dicentrics (Benarroch-Popivker et al., 2016; Lescasse et al., 2013; Reis et al., 2012; van Steensel et al., 1998). Finally, mechanisms ensure that epigenetic centromeres do not form at the wrong locations (Müller and Almouzni, 2017). However, there are contexts where dicentrics occur more frequently. The first described is exposure to ionizing radiations (Muller and Altenburg, 1930). Generating multiple and simultaneous double-strand breaks, they favour erroneous NHEJ repair between breaks, giving rise to dicentric and acentric chromosomes at a remarkably high frequency (Kaddour et al., 2017; M'kacher et al., 2014; Suto, 2016). Human oncogenesis is another context where dicentric occurrence is prevalent. In cells having bypassed senescence, extensive telomere shortening results in frequent end-to-end fusions and dicentric chromosomes. This leads to transient but substantial genome instability from which can emerge malignant cells with mutations and gene copy number alterations allowing an escape from the controls preventing cancer (Maciejowski and de Lange, 2017).

Some cells can circumvent the genome instability that would otherwise result from telomere fusions. In *Saccharomyces cerevisiae*, dicentrics formed by telomere fusions most often break at the fusion. This process restores the parental chromosomes and allows cell lineages to recover from fusions with a normal karyotype (Pobiega and Marcand, 2010). Thus, a backup rescue pathway can protect cells from the adverse consequences of accidental telomere fusions. Our current understanding of telomeres does not provide obvious hypotheses to explain how telomere fusions in dicentrics are more prone to breakage.

In *S. cerevisiae*, dicentrics lacking telomere fusion break with greater likelihood near centromeres (López et al., 2015; Song et al., 2013). Whether it occurs at telomere fusions, at pericentromeres or somewhere in-between centromeres, the severing of dicentrics does not occur in response to chromatin stretching. Instead, dicentric breakage requires cytokinesis (López et al., 2015). Preferential breakage at pericentromeres or telomere fusions may result from their preferential entrapment by the closing septum. In agreement with this model, dicentric centromeres rapidly converge toward each other by an unknown mechanism after spindle disassembly and the onset of cytokinesis (López et al., 2015). This movement brings the centromeres and the intercentromeric chromatin in close proximity to the plane of cytokinesis. It could involve condensin, the loop-extruding motor required for chromosome arm segregation and telomere disjunction in anaphase (Ganji et al., 2018; Lazar-Stefanita et al., 2017; Renshaw et al., 2010; Reyes et al., 2015; Sun et al., 2018).

Here we addressed what causes the preferential breakage of dicentrics at telomere fusions and the rapid movement of dicentric centromeres following the onset of cytokinesis. We found that simple arrays of closely spaced binding sites for the telomere-binding factor Rap1 or the heterologous high-affinity DNA-binding factor lacI are sufficient to mimic the breakage hotspot established by telomere fusions within dicentrics. Condensins drive the dicentric-induced post-anaphase recoiling and are essential for dicentric breakage at centromere-proximal regions. Preferential breakage at Rap1-bound arrays also requires condensin. Together these results show that preferential breakage at telomere fusions is the consequence of a condensin-driven chromosome folding that is imposed by the tight binding of Rap1 to DNA and favours entrapment by the septum at the completion of cytokinesis.

Results

Dicentrics preferentially break at internal telomeres

Telomere fusions shown to be more prone to breakage within dicentrics are head-to-head fusions of telomere repeats flanked by the native subtelomere sequences (Pobiega and Marcand, 2010). The palindromic structure of the fusion, the telomere and subtelomere sequences as well as factors bound to them could be important in creating a breakage hot spot. We initially asked whether non-palindromic internal telomere repeats within a dicentric chromosome are also more prone to breakage.

To study dicentric breakage, we created conditional dicentric chromosomes with a conditional centromere (Hill and Bloom, 1989; López et al., 2015). In short, the native centromere of chromosome 6 (*CEN6*) is flanked by two galactose-inducible promoters. On galactose, *CEN6* is mostly inactive and detached from the kinetochore microtubule. When transcription is turned off by glucose, the centromere is rapidly reattached to a microtubule and its function is restored (Tanaka et al., 2005). Fusing by homologous recombination the end of chromosome 6 right arm (6R) to the end of chromosome 7 left arm (7L) generates 6+7 dicentrics whose centromeres are 600 kb apart (Figure 1B, Supplemental Figure S1A). These conditional dicentrics are stably propagated as long as *CEN6* is inactivated by galactose. First, we tested two configurations of 6+7 dicentrics: one lacking internal telomere repeats and one with 300 bp of direct (non-palindromic) TG_{1-3} telomere repeats inserted at the junction between the two fused chromosomes. Both dicentrics have lost the native 7L subtelomere and kept the native 6R subtelomere.

To look at dicentric breakage during a single cell cycle, cells grown in the presence of galactose were synchronized in G1 and released from the arrest in a glucose-containing medium. Cells were either blocked at the G2/M transition or allowed to progress through mitosis until they were blocked again in the next G1. Intact and broken chromosomes were separated by pulse-field gel electrophoresis (PFGE) and hybridized with a probe from one side of the dicentric. In the absence of internal telomere repeats, pericentromeres are the preferred breakage positions (Figure 1C), as previously observed (López et al., 2015). The insertion of direct telomere repeats is sufficient to create a hot spot of breakage (Figure 1C). This shows that the head-to-head palindrome formed by the fusion is not essential in favouring dicentric breakage. Note that in cells arrested prior to mitosis (G2/M), a fraction of the dicentric molecules are already broken at the position where internal telomeres are inserted. This background of

breakage stems mostly from residual *CEN6* activity in a galactose-containing medium (Supplemental Figure S1B) (Pobiega and Marcand, 2010).

Dicentrics preferentially break at Rap1-bound tandem arrays

Yeast TG_{1-3} telomere repeats are arrays of high affinity binding sites for the Rap1 protein (Wellinger and Zakian, 2012). To assess whether Rap1 binding in tandem is what creates a dicentric breakage hotspot, we inserted tandem arrays of 6 to 24 Rap1 binding sites within a 6+7 dicentric lacking both 6R and 7L subtelomere sequences. We chose high-affinity sites with close spacing known to mimic Rap1 binding density at native telomere sequences (14 bp site with alternate spacers of 1 and 6 bp) (Grossi et al., 2001; Williams et al., 2010). As shown in Figure 1D, dicentric breakage occurs preferentially at multiple Rap1 binding sites. A tandem of 6 sites is sufficient to pass the detection threshold. Increasing the number of Rap1 sites strengthens breakage at the array and concomitantly weakens breakage at pericentromeric regions. Thus, tandem arrays of high affinity Rap1 binding sites are sufficient to establish a hotspot of breakage within a dicentric in the absence of adjacent subtelomere sequences.

To test whether the position of the Rap1 sites within a dicentric influences their ability to establish a breakage hotspot, we compared the impact of a 16 Rap1 binding sites array inserted closer to one centromere (1/6) or halfway between the centromeres within chromosome 7 left arm (1/2). As shown in Figure 1E, breakage frequencies at these inserted positions are indistinguishable. This shows that the ability of Rap1 sites to establish a breakage hotspot is largely independent of the surrounding chromatin environment.

Next, we asked whether Rap1 binding to its sites is essential to establish a breakage hotspot. Since Rap1 is also a transcription factor essential for viability (Candelli et al., 2018; Knight et al., 2014; Kubik et al., 2018; Lickwar et al., 2012), we used two complementary approaches to address this issue. First, we tested a tandem array of 28 mutated sites with base changes disrupting the Rap1 consensus binding site, while conserving its G-richness. This array is unable to establish a hotspot of breakage (Figure 1F). Second, we assessed where a dicentric with internal telomere repeats breaks when the Rap1 level is reduced approximately 10-fold with the help of an inducible degron (Supplemental Figure S1C). A lower Rap1 level decreases breakage specifically at internal telomere repeats, not near centromeres (Supplemental Figure S1D). Together

these results indicate that tandem arrays bound by Rap1 are sufficient to establish a breakage hotspot within a dicentric chromosome.

Dicentrics preferentially break at lacO arrays bound by lacI

We then asked how Rap1 can impact dicentric breakage. At telomeres, Rap1 recruits the Rif1, Rif2, Sir3 and Sir4 proteins, which are important for telomere protection and telomere length homeostasis (Wellinger and Zakian, 2012). In cells lacking one or several of these proteins or the associated protein Sir2, internal telomere repeats still generate a dicentric breakage hotspot (Supplemental Figure S3A), showing that they are not essential to this process. Since Sir2, Sir3 and Sir4 are essential yeast heterochromatin components, it also rules out heterochromatin as the structure favouring dicentric breakage at internal telomere repeats.

A hallmark of Rap1 is to bind its sites with a high affinity (K_D ~20 pM) (Matot et al., 2012; Williams et al., 2010). For instance, this property allows Rap1 to roadblock RNA PolII transcription (Candelli et al., 2018; Challal et al., 2018). If tight Rap1-DNA interaction is sufficient to establish a dicentric breakage hotspot, its effect should be mimicked by other tight DNA binders. We tested this hypothesis with a heterologous DNA-binding protein, lacI, known for its high affinity to its site lacO (K_D ~10 pM (Falcon and Matthews, 1999)). Arrays of lacO were inserted within a dicentric. As shown in Figure 2A, an unbound array of 200 lacO or the same array bound by a mutant lacI with a reduced DNA binding affinity (lacI** (Dubarry et al., 2011), see materials and methods) do not impact dicentric breakage. By contrast, the same array of 200 lacO bound by a lacI protein with high DNA binding affinity (lacI) establishes a breakage hotspot. Its intensity is severely diminished by addition of isopropyl ß-D-1-thiogalactopyranoside (IPTG), which lessens lacI affinity to its site. Reducing the size of the lacO array also weakens the hotspot (Figure 2B). Finally, in the absence of lacO, lacI has no impact on dicentric breakage. Thus, a tandem array tightly bound by a heterologous protein is sufficient to mimic the ability of multiple Rap1 binding sites to favour dicentric breakage nearby. This suggests that the key Rap1 property in this process is to tightly bind its sites in tandem.

How tight protein-DNA interactions may directly favour dicentric breakage is unclear. They might be important at the time of breakage at the end of cytokinesis. By challenging replication fork progression (Dubarry et al., 2011; Goto et al., 2015; Koc et

al., 2016), they may also leave a mark in S phase that later influences where dicentrics are severed by cytokinesis. Inhibiting the lacI-lacO interaction with IPTG offers an opportunity to test the latter hypothesis. As shown in Figure 2C, when IPTG is added after S phase to cells released from a G2/M arrest, preferential breakage at the lacO array is lost. By contrast, when cells are exposed to IPTG during S phase only until G2/M (a situation where array replication will not be challenged by tight binding), breakage at the lacO array during mitosis is as frequent as in cells unexposed to IPTG. This lacO array is adjacent to an early replication origin (*ARS707*) (Müller et al., 2014) and previous works showed that tightly bound lacO arrays can replicate early in S phase (Ebrahimi and Donaldson, 2008; Ebrahimi et al., 2010). These results indicate that lacI interaction during progression through mitosis is sufficient for the establishment of a dicentric breakage hotspot at a lacO array, irrespective of its interaction during S phase. Thus, replication challenges at the bound array are unlikely causes for preferential breakage within dicentrics. The question remains as to what structure created by protein-bound tandem arrays favours breakage. To address this issue, we next asked which step of cytokinesis is essential to sever dicentrics.

Dicentric breakage only requires septation, not the actomyosin ring contraction or the following cell separation

During yeast cytokinesis, the contraction of an actomyosin ring guides septation. Once contracted to a 100-200 nm diameter, the ring disassembles to allow the further growth of the septum to fill the remaining hole (Bi and Park, 2012; Onishi et al., 2013; Weiss, 2012). Our previous observations by transmission electron microscopy showed that, in cells with a dicentric, the closing septum can pinch the nuclear envelope (López et al., 2015). This can also be seen at lower resolution by time-lapse microscopy in live cells where histones and the plasma membrane are labelled with fluorophores (Figure 3A, Supplemental Figure S3B). In cells where dicentric anaphase bridges are formed, the two nuclei are connected and are abnormally close to each other at the time of ingression and separate shortly after. Although diffraction prevents a precise definition of the timing of abscission completion, the two events seem coincident with our time resolution. This (and similar observations by (Amaral et al., 2016)) further suggests that breakage is induced after ring disassembly by septum closure. Therefore, dicentric breakage should only require septation but not the preceding ring contraction or the

following cell separation. To test this prediction, we first looked at breakage in a context where cytokinesis is independent of the actomyosin ring.

In the absence of the myosin Myo1, the actomyosin ring is not assembled and septation is significantly impaired. Myo1 depletion with an auxin-inducible degron (*myo1-AID* + IAA) results in a sharp decrease in dicentric breakage at pericentromeres (Figure 3B left panel, as reported previously (López et al., 2015)) and at a Rap1-bound tandem array (Figure 3B right panel). Cells completely lacking Myo1 (*myo1-Δ*) grow very poorly due to frequent failure at cytokinesis. Upon continuous selection, they acquire mutations and gene copy number changes that promote cell wall biogenesis and restore an efficient and timely cytokinesis through the growth of a compensatory septum in the absence of a contractile actomyosin ring (Bi et al., 1998; Rancati et al., 2008) (Supplemental Figure S3B). Conditional dicentrics were created in these adapted *myo1-Δ* cells carrying out cytokinesis only through septation. As shown in Figure 3B (left and right panels), dicentric breakage occurs in *myo1-Δ* cells as in wild-type cells. Therefore, septation is sufficient to sever dicentrics and actomyosin ring contraction can be bypassed.

Next, we asked whether cell separation contributes to dicentric breakage. Following abscission, degradation and rearrangement of polysaccharide chains within the septum allow cell separation. The transcription factor Ace2 activates the expression of genes encoding septum remodelling enzymes carrying out this process. Its absence prevents or severely delays cell separation (Brace et al., 2019; Voth et al., 2005; Weiss, 2012). In cells lacking Ace2, dicentrics break as in normal cells (Figure 3C, left and right panels). We conclude that breakage does not need the post-abscission septum remodelling leading to cell separation. Together these results further support the hypothesis that septum closure severs dicentrics. Two scenarios can be postulated. The lateral forces applied by septum closure could be sufficient to cause DNA cleavage. Alternatively, a nuclease could cleave DNA in response to septum closure. The implication of a nuclease is reminiscent of recent observations in animal cells. In human cells, the cytosolic exonuclease TREX1 can enter a ruptured nucleus and process dicentric bridges (Maciejowski et al., 2015). In *Caenorhabditis elegans*, the endonuclease LEM-3[Ankle1] is brought to DNA bridges by actomyosin contraction and contributes to their resolution (Hong et al., 2018a). These nucleases have no known ortholog in yeast. Instead, we tested the implication of Yen1 and Mus81, two endonucleases active in late mitosis and

implicated with LEM-3 in the resolution of recombination intermediates in *C. elegans* (Hong et al., 2018b). Their absence in yeast does not prevent dicentric breakage (Supplemental Figure S3C), indicating that unidentified nucleases or physical forces break DNA at abscission.

Centromeres relocation to the bud neck and breakage near centromeres require condensin

Dicentric anaphase bridges cause a relocation of the centromeres and the centromere-linked spindle pole bodies (SPB, yeast's centrosome equivalent) towards the bud neck during septation (Amaral et al., 2016; López et al., 2015; Thrower and Bloom, 2001) (Figure 4A, bottom panel; Supplemental Figure S4A). This movement occurs relatively late during cytokinesis, often after actomyosin ring disassembly (López et al., 2015). In cells without dicentric, SPBs also relocate at this time, but only slightly to the cell middle, not to the bud neck (Figure 4A, top panel; Supplemental Figure S4B). The initial trigger is likely to be the same event in both cases, mitotic spindle disassembly or SPB release from an attachment to the cell cortex. In the absence of chromatin bridges, the nuclei and the SPBs regain their position in the middle of the cell. In the presence of dicentric bridges, recoiling of the stretched chromatin into a non-stretched state would cause rapid SPB relocation to the bud neck. In addition, active chromatin compaction by condensin could contribute to this process (Ganji et al., 2018; Lavoie et al., 2004; Lazar-Stefanita et al., 2017; Renshaw et al., 2010). To test the role of condensin in dicentric centromere relocation, we created a conditional 6+7 dicentric in cells carrying an auxin-inducible degron of Smc2, a SMC subunit of yeast condensin (Supplemental Figure S4C&D).

First, we monitored SPBs movement during the mitosis that follows *CEN6* reactivation and auxin (indole-3-acetic acid or IAA) addition (Figure 4B, Supplemental Figure S5). As previously observed, in a wild type context, SPBs snap back towards each other at the end of furrow ingression in nearly half the cells with a dicentric, the fraction where anaphase bridges are formed. Interestingly, SPB snap back is often asymmetrical with one pole moving to the bud neck before the other (Supplemental Figure S4E), suggesting that the movement trigger is an event that can impact one of the SPB earlier than the other (for instance an earlier release from cell cortex attachment or a precocious recoiling in one nuclear lobe). In Smc2-defective cells, the frequency of

dicentric-induced SPBs snap-back is markedly decreased (p<0.001 χ^2 with a threshold for the shortest SPB-SPB distance at 2 μm) (Figure 4B). In cells without dicentric, Smc2 loss does not change the SPB dynamics.

Second, we tracked the position of one centromere in a dicentric using a lacO array inserted near *CEN7* and bound by a low-affinity GFP-lacI** mutant (Figure 4C). To estimate the relocation of the centromere toward the bud neck, we measured the shortest observed distance between the lacO array and the plan of cytokinesis after actomyosin ring contraction with a time resolution of 2 minutes. In wild type cells without dicentric this distance is in most cases larger than 1 μm, whereas in cells with a dicentric, it is frequently shorter than 1 μm (Figure 4D). When Smc2 is degraded, cells where the shortest distance passes below this threshold are less frequent (p<0.01 χ^2). In other words, a condensin defect allows dicentric centromeres to remain away from the bud neck at the time of abscission. Together, these results show that condensins are required to the dicentric-induced relocation of the SPBs and the centromeres. Thus, this sudden movement likely results from an active chromatin compaction of the stretched chromatin bridges, a process dragging along the centromeres and the attached SPBs towards the plane of cytokinesis prior to breakage.

If breakage results from DNA entrapment at the bud neck when cytokinesis is completed, an inability to relocate centromeres nearby should prevent breakage in the pericentromeric regions. To test this prediction, we looked at breakage in Smc2-depleted cells. As shown in Figure 4E, condensin loss strongly reduces breakage near centromeres and concomitantly favours breakage in the middle part of the intercentromeric region. Since centromeres remain away from the bud neck in condensin defective cells, breakage frequency correlates with bud neck proximity when the septum closes. This indicates that chromatin can only be severed near where abscission takes place. It also shows that, in wild-type cells, breakage occurs after dicentric refolding.

Breakage near centromeres in shorter dicentrics still requires condensin

To further explore the importance of chromosome condensation on dicentric breakage positions, we addressed the severing of dicentrics with shorter distances between centromeres for which the dependence on condensin could be less pronounced. In this setting, a short fragment carrying a centromere is inserted in

chromosome 6 at either 100 or 45 kb from the conditional *CEN6* centromere. In wild type cells, the ectopic centromere establishes a hotspot of breakage indistinguishable from the hotspot adjacent to native centromeres (López et al., 2015) (Figure 5A). In *smc2-AID* cells depleted of Smc2 by IAA addition, breakage positions move away from the centromeres toward the median part of the dicentrics. Interestingly, breakage at centromeres is less frequent in untreated *smc2-AID* cells (-IAA) compared to wild type cells, indicating that condensin function is already partially impaired in non-induced conditions (a similar but less pronounced shift is noticeable with longer dicentrics, Figure 4E). In conclusion, condensin are essential to break in pericentromeric regions even when the centromeres are relatively close to each other.

Preferential breakage at Rap1 sites requires condensin

We then asked whether preferential breakage at a Rap1-bound tandem array requires condensin. When Rap1 sites are inserted closer to one of the centromeres (relative position 1/6, intercentromeric distance 600 kb), Smc2 loss strongly diminishes breakage frequency at the Rap1 sites (Figure 5B). This indicates that condensins are essential to the establishment by Rap1 of a breakage hotspot, at least when the Rap1 sites are off-centre. However, Rap1-bound arrays could remain a breakage hotspot in condensin-defective cells when located within the middle part of the intercentromeric region where breakage now mostly occurs. Therefore, we next tested if a Rap1-bound tandem array located within this middle region is still preferentially severed in the absence of condensin.

In cells where tandem Rap1 sites are inserted halfway between the centromeres of 6+7 dicentric (relative position 1/2), breakage positions relocate to the middle part of the intercentromeric region in response to condensin loss (Figure 5C). The overlap with the Rap1 sites conceals the change in breakage frequency that may occur at the Rap1 sites. To circumvent this limitation, we established a stronger hotspot in a shorter dicentric (Figure 5D). In this setting, chromosome 6 right arm is fused to the right arm of chromosome 1 with or without a cloned telomere fusion of ~400 bp at the junction. The distance between the fusion and *CEN6* or *CEN1* is ~120 kb and ~80 kb respectively. In wild-type cells, the telomere fusion establishes a strong breakage hotspot. In the absence of telomere fusion, breakage occurs more frequently in the pericentromeric regions and relocates to the middle part of the intercentromeric region in condensin-

defective cells (Figure 5D). When the telomere fusion is present, condensin loss also causes a marked reduction of breakage at the fusion (Figure 5D). Breakage at fusion is less frequent in untreated *smc2-AID* cells (- IAA) compared to wild type cells, consistent again with a partial condensin loss of function in non-induced conditions. Thus, preferential breakage at a Rap1-bound array requires condensin even when the array is located within the median region where dicentrics break in condensin-defective cells.

Close spacing between tandem Rap1 sites is essential to establish a breakage hotspot

The preferential breakage at Rap1-bound arrays appears as the consequence of a propensity to be entrapped at the abscission site when cytokinesis is completed. Since this preferential entrapment is also condensin-dependent, it may be due to a constraint imposed by Rap1 binding on condensin activity. One hypothesis is that Rap1-bound arrays can stall condensin activity by outcompeting DNA binding over the entire tandem arrays. A prediction of this model is that increasing the distance between the bound molecules should allow condensin to bind within the array and to pass through it unchallenged.

To address this hypothesis, we inserted a tandem array of 16 interspaced Rap1 binding sites within a 6+7 dicentric. In this setting, 8 clusters of two closely spaced Rap1 sites are separated by larger 35 bp linkers whose sequences harbour a single lacO site (Figure 6A; in the control closely spaced array, successive sites are separated by 1 or 6 bp). As shown in Figure 6B, this interspaced array in the absence of lacI fails to establish a breakage hotspot, indicating that a close spacing of the Rap1 sites is essential to impact dicentric breakage. Interestingly, lacI presence transforms the same array into a strong breakage hotspot. This property requires high affinity of lacI for its site, since reducing this affinity with IPTG weakens the hotspot (Figure 6B), again indicating the importance of a close spacing of tightly bound proteins on DNA to favour breakage within a dicentric. These results match our initial hypothesis that Rap1 acts through a stalling of condensin by steric hindrance.

Finally, the impact of tightly bound arrays on condensin could be associated to changes in tri-dimensional chromosomal folding, as seen previously for the rDNA at the scale of chromosome 12 (Lazar-Stefanita et al., 2017). To test whether Rap1- or lacI-bound arrays alter chromosome conformation, we applied chromosome conformation capture (Hi-C) to cells without dicentric arrested in late anaphase. The binding of lacI

reduces the contact frequencies between sequences positioned on either side of the lacO array, but whether Rap1 can exert a similar insulating effect is less clear (Supplemental Figure S6A&B). The sensitivity of the Hi-C assay combined with the limited mappability of the sequenced reads on these repeated regions might be a limiting factor (Swygert et al., 2018). For instance, the frequent short-range *cis*-contact events involving short-range distances may generate noise concealing the detection of condensin-dependent contacts that would be impacted by Rap1. In support of this interpretation, condensin loss has no obvious impact on short-range (<~50 kb) contact frequencies over the entire genome (Supplemental Figure S6C&D), although chromosome 12 loses its conformation as described (Lazar-Stefanita et al., 2017). Methodological developments or alternative approaches will be needed to further explore this issue.

Discussion

This study shows that the preferential breakage of dicentrics at internal telomere sequences in yeast depends on condensin, septation and tight Rap1 binding. It addresses the molecular mechanism of a unique rescue pathway protecting cells from the detrimental consequences of telomere fusions. Furthermore, it has implications for our understanding of chromosome condensation and telomere function.

Condensin-driven dicentric recoiling

Dicentric anaphase bridges recoil just prior to breakage at the completion of cytokinesis (Figure 7A). Our findings reveal that this recoiling of stretched chromatin fibres requires condensin, the SMC protein complex compacting chromosome in mitosis (Cheng et al., 2015; Ganji et al., 2018; Gibcus et al., 2018; Kschonsak et al., 2017; Lazar-Stefanita et al., 2017; Nasmyth, 2017; Renshaw et al., 2010; Shintomi et al., 2017). This shows that condensin remains active until the end of mitosis and that extensive chromosome compaction by condensin is not restricted to the rDNAs in yeast, as originally thought (e.g. (Hirano, 2017)). It extends previous observations on condensin-dependent recoiling of yeast chromosome arms in early anaphase (Renshaw et al., 2010) and unambiguously shows that condensin can generate forces sufficient to pull and rapidly compact yeast chromatin severalfold *in vivo*.

During anaphase, the elongated spindle and possibly the SPB attachment to the cell cortex oppose the condensation of dicentric bridges. Once these antagonists expire, compaction is restored through the same protein complex that condenses chromosome arms earlier in mitosis. This adaptability likely depends on the observed dynamic interaction between condensin and chromatin *in vivo*, with frequent loading and unloading (Renshaw et al., 2010; Robellet et al., 2015; Thadani et al., 2018; Thattikota et al., 2018). From anaphase onset through the completion of cytokinesis, condensin-dependent chromatin loops may constantly form and come apart to establish a steady-state level of compaction. The recoiling of dicentric bridges would therefore be a return to equilibrium that manifests an activity present on all chromosome arms at this time.

In vitro, yeast condensin extrudes loops of naked DNA at rates up to ~1 kb per second (Ganji et al., 2018). At this rate, the observed recoiling of 600 kb dicentric bridges in less than a few minutes (Figure 4) would require the combined action of only a few condensin molecules. However, loop extrusion velocity might be different on nucleosomal fibres. It may also be reduced by counteracting forces, as observed *in vitro* (Ganji et al., 2018). In addition, the initial stretching of chromatin may impact condensin recruitment and activity. Finally, condensin activation might be distinctively regulated at this late stage of mitosis compared to earlier in anaphase. For instance, it could depend on Ipl1[Aurora B] (Lavoie et al., 2004). Dicentrics will be attractive tools to address these issues in live cells.

Interestingly, condensins acting on dicentric chromatids are strong enough to pull along the SPBs and through them the other chromosomes within the nucleus. Since this movement is relatively slow at a molecular scale (10-100 nm/s), the force needed to oppose the viscous drag is likely small (i.e. <1 pN) (Bloom, 2007). Therefore, it should not be a challenge to the kinetochore-microtubule connection, whose strength is estimated at ~10 pN (Miller et al., 2016) and is compatible with the known strength of single condensin molecules, which *in vitro* can oppose tension on DNA up to 2 pN (Eeftens et al., 2017; Ganji et al., 2018).

Preferential entrapment of pericentromeres and Rap1/lacI-bound arrays

Condensin loss prevents the relocation of centromeres to the bud neck at the end of septation (Figure 7B). As a consequence, it prevents the severing of dicentrics near centromeres and favours breakage in the median region, linking the spatial proximity to

the bud neck at the time of abscission to the probability of being severed by septation. Thus, dicentric breakage hotspots result from a higher chance to be entrapped at the abscission site.

Preferential entrapment may stem from a condensin-dependent particular conformation or from an asymmetric distribution of chromatin. When the closing septum entraps the pericentromeric region of a dicentric, the intercentromeric chromatin is entirely folded in one nuclear lobe (Figure 7A). A simple symmetry breaking could be sufficient to explain this end point. For instance, if condensin recruitment and loop extrusion are distributed randomly on chromatin and remain dynamic, small fluctuations in favour of one nuclear lobe could increase chromatin density and therefore the likelihood of further condensin recruitment and loop extrusion within it, establishing a positive feedback tending to fold the entire intercentromeric region in one nuclear lobe. Further chromosome translocation beyond the centromere could then be impeded by a bulky kinetochore unable to pass through the narrow hole left at the closing neck. The centromere connected to the kinetochore could also directly stall loop-extrusion by condensin. In both cases, it will favour the entrapment of the pericentromeric regions at the closing neck. Note that the proposed positive feedback should also promote full arm compaction of monocentric chromosomes in one nuclear lobe, thereby contributing to an efficient segregation in normal cells.

Can a similar model explain the frequent entrapment of Rap1 site tandem arrays, including telomere fusions? Since Rap1 effect can be mimicked by the heterologous DNA binding factor lacI, its key attribute in this process is that it binds DNA tightly with close spacing. In addition, the preferential entrapment of Rap1-bound arrays depends on condensin, indicating that Rap1 may act by impacting condensin activity (Figure 7C, D). One possibility is that, as suggested for the rDNA (Lazar-Stefanita et al., 2017), Rap1-bound arrays create a roadblock for condensins (Supplemental Figure S7A). How condensin acts is as yet unknown but it may proceed through the recurrent formation of small intermediate loops, each one involving multiple condensin contacts with DNA and short-range DNA bending (Diebold-Durand et al., 2017; Ganji et al., 2018; Kschonsak et al., 2017; Marko et al., 2018) (Supplemental Figure S7B). Rap1/lacI bound on high-affinity sites in tandem with a close spacing may antagonize condensin-DNA interactions by steric hindrance, thereby impeding loop extrusion through the bound arrays.

Increasing the spacing between the bound sites would release condensin from this impediment (Supplemental Figure S7B). In addition, Rap1 binding on tandem arrays is known to stiffen DNA *in vitro*, generating stick-like structures that would be, for 16 sites in tandem, longer than condensin (~100 nm vs ~50 nm) (Le Bihan et al., 2013). This stiffening may also oppose the transient bending required for loop extrusion, although this too remains to be determined. Condensin stalling at a bound tandem array could promote independent folding of each side of the array in the two nuclear lobes or perhaps a local decondensation around the array that in the context of a dicentric would favour its entrapment at the abscission site (Figure 7C, D). An alternative model for condensin proposes loop formation by stochastic pairwise interactions reinforcing spatial proximity and therefore condensation (Cheng et al., 2015). It would be interesting to explore whether Rap1/lacI-bound arrays could also challenge this self-reinforcing mechanism. The impact of condensin stalling at native telomeres also has yet to be addressed. Finally, the impact of high-affinity lacI also advocates the use of a low-affinity lacI allele when using lacO arrays to track chromosome mobility, as previously recommended (Dubarry et al., 2011).

Breakage by septum closure

Once DNA is entrapped at the abscission site, how can cytokinesis sever it? Actomyosin ring contraction and the post-abscission septum remodelling leading to cell separation are not needed for dicentric breakage. The severing of DNA is likely to result from the closing septum pinching the nucleus and the dicentric bridges. An unidentified nuclease could be brought or activated by septation. An alternative scenario is that physical shearing forces are sufficient to break DNA entrapped at abscission. These forces could stem from the growth of the polysaccharide chains that build the septum, approximately a few tens of pN for each sugar monomer added (Cabib and Arroyo, 2013; Proctor et al., 2012). If dicentric bridges are transiently embedded into this dynamic, dense and crosslinked network, the forces from the motion of individual chains could apply stochastically on the DNA molecule at multiple points and be additive to some extent, as in a linear random walk model. This would be sufficient to generate shearing forces above the few hundred pN needed to break covalent bonds in the DNA backbone. In this scenario, dicentric bridges would rapidly shear off once the septum has closed on them. DNA severing by shearing forces could be ubiquitous in species with a septum

such as budding yeasts, fission yeasts and bacteria, all known to break lagging chromatin at cytokinesis (Baxter and Diffley, 2008; Cuylen et al., 2013; Hirano et al., 1986; Hocquet et al., 2018; Quevedo et al., 2012). In addition, shearing forces could break other accidentally entrapped macromolecules that could otherwise challenge abscission. Relying on physical forces would be an effective way to proceed since the lack of chemical specificity would allow this mechanism to act regardless of the nature of the hindrance. It will be thought provoking to explore this hypothesis.

Author Contributions

Conceptualization, T.G. and S.M.; Methodology, T.G., R.K., K.D. and S.M.; Investigation & Validation, T.G., C.B, N.B., V.L., L.L.S., A.D., A.T. and S.M.; Supervision, R.K. and S.M.; Project Administration, S.M.; Funding Acquisition, R.K., K.D. and S.M.; Writing Original Draft, S.M.; Writing – Review & Editing, T.G., C.B., R.K., K.D. and S.M.

Declaration of Interests

The authors declare no competing interests.

Figure legends

Figure 1: Preferential dicentric breakage at Rap1 bound tandem arrays. (**A**) Segregation of a dicentric formed in G1. In Anaphase, the two centromeres of each sister chromatid can migrate to the same pole, thus propagating the dicentric intact to the next generation in the two offspring. Alternatively, the centromeres of each sister chromatid can migrate to opposite poles, forming two anaphase bridges, which are severed at cytokinesis. (**B**) Fusion of chromosome 6 right arm to the left arm of chromosome 7 by homologous recombination. (**C**) Preferential breakage at internal telomere repeats. Cells having a 6+7 dicentric, with or without 300 bp of telomeric repeats inserted at the junction between chromosomes 6 and 7, were grown exponentially in galactose-containing medium, synchronized in G1 with α-factor, released in glucose-containing medium and either blocked in G2/M with nocodazole (G2/M) or allowed to proceed through mitosis to be blocked in the next G1 with α-factor (next G1). Chromosomes were separated by PFGE (left panel, gel red labelled) and probed with a fragment from chromosome 6 left arm (right panel). (**D**) Preferential breakage at internal arrays of Rap1 binding sites. The experiment was performed as above with cells possessing a 6+7 dicentric with 0 to 24 Rap1 binding sites in tandem inserted at the junction between chromosomes 6 and 7. The upward smear at Rap1 arrays is likely due to partial 5' resection of the broken ends in G1-arrest cells (López et al., 2015). (**E**) Preferential breakage at Rap1 binding sites inserted in-between centromeres. Cells possess a 6+7 dicentric with no inserted Rap1 site (-), 16 Rap1 binding sites inserted at the junction between chromosomes 6 and 7 (1/6) or 16 Rap1 binding sites inserted within chromosome 7 left arm (1/2). (**F**) Lack of breakage at mutated Rap1 sites. Cells possess a 6+7 dicentric with no inserted Rap1 site (-), 24 Rap1 binding sites (24) or 28 mutated sites unable to bind Rap1 (28 mut.). Both tandem arrays are inserted at the junction between chromosomes 6 and 7. Rap1 site: GG**T**GT(C/A)TGGG**T**GTA . Mutated site: GG**A**GT(C/A)TGGG**A**GTA. Gel Red labelled PFGE shown in Supplemental Figure S2.

Figure 2: Preferential dicentric breakage at lacO arrays bound by lacI. (**A**) Breakage at a lacO array bound by lacI. Cells proceeded through mitosis with or without 2mM IPTG. Cells possess a 6+7 dicentric with 200 lacO sites inserted within chromosome 7 left arm. Low-affinity lacI** and high-affinity lacI are expressed from an integrated plasmid. (**B**) Breakage at a lacO array depends on the array size. Cells expressing lacI possess a 6+7 dicentric with 0 to 200 lacO sites. (**C**) Breakage at a lacO array requires lacI binding during progression through mitosis. Cells possessing a 6+7 dicentric with

200 lacO sites and either an empty vector (-) or a integrated plasmid expressing lacI (lacI) were released in glucose from G1 with or without IPTG and either blocked in G2/M with nocodazole (G2/M) or allowed to proceed to the next G1 (next G1). Cells blocked in G2/M were released with or without IPTG and blocked in the next G1 (next G1 from G2/M arrest). Gel Red labelled PFGE shown in Supplemental Figure S2.

Figure 3: Dicentric breakage by septation. (**A**) Dicentric-induced chromatin pitching by septation. Cells possessing a dicentric 6+7 without inserted tandem array were grown exponentially at 30°C in galactose-containing medium and switch to glucose 30 minutes before imaging at 30°C. One image taken every minute. Plasma membrane is labelled with TTyeGFP-Spo20[51-91] and nucleosomes with a HTA1-mCherry tag. Scale bar, 1μm (pixel size 52 nm). The scheme on the left represents the chromatids (grey) conformation that does not create (upper image) or creates (lower image) an anaphase bridge. (**B**) Dicentrics still break in cells carrying out septation without a contractile actomyosin ring. WT, *myo1-AID* and adapted *myo1-Δ* cells possessing a 6+7 dicentric with no inserted Rap1 site (-) or an array of 24 Rap1 binding sites inserted at the junction between chromosomes 6 and 7 (24 Rap1 sites) proceeded through mitosis with or without 2mM IAA. (**C**) Dicentrics still break in cell-separation defective cells. WT and *ace2-Δ* cells possessing a 6+7 dicentric with no inserted Rap1 site (-) or an array of 24 Rap1 binding sites inserted at the junction between chromosomes 6 and 7 (24 Rap1 sites) proceeded through mitosis with or without 2mM IAA. Gel Red labelled PFGE shown in Supplemental Figure S2.

Figure 4: Centromere relocation to the bud neck and breakage near centromeres require condensin. (**A**) Example of dicentric-induced SPBs relocation to the bud neck shortly after cytokinesis onset. Wild-type cells possessing a 6+7 dicentric without inserted tandem array were grown in galactose-containing medium and switched to glucose 30 minutes before imaging at 30°C. One image taken every two minutes. Plasma membrane is labelled with TTyeGFP-Spo20[51-91] and the SPBs with a Spc42-mCherry tag. Scale bar, 1μm (pixel size 65 nm). Upper panel: example of normal (monocentric-like) SPBs dynamics during septation. Lower panel: example of dicentric-induced SPBs snap-back during septation. (**B**) Condensin depletion reduces the frequency of the dicentric-induced SPBs snap-back. TTyeGFP-Spo20[51-91] Spc42-mCherry wild-type and *smc2-AID*

cells possessing a dicentric 6+7 were grown in galactose-containing medium and switch to glucose 30 minutes with or without 2mM IAA before imaging at 30°C. Monocentric cells were directly imaged in glucose-containing medium with or without 2mM IAA. For each condition, the shortest distance between the two SPBs reached during the four minutes following ingression onset is plotted. Data from individual cells are showed in Supplemental figure S6. (**C**) Example of dicentric-induced centromere relocation to the bud neck shortly after cytokinesis onset. Wild-type cells possessing a 6+7 dicentric were imaged as in A. The contractile actomyosin ring is labelled with a Myo1-GFP tag, the SPBs with a Spc42-mCherry tag and the *CEN7* centromere with a lacO array inserted ~15 kb from *CEN7* and bound by a low-affinity GFP-lacI**. Upper panel: example of normal (monocentric-like) centromere dynamics. Lower panel: example of dicentric-induced centromere relocation. (**D**) Condensin depletion allows dicentric centromeres to remain more often away from the bud neck after ingression onset. Wild-type and *smc2-AID* cells either monocentric or possessing a 6+7 dicentric were imaged as in B. For each condition, the shortest distance between the lacO spots and the position of Myo1 reached during the four minutes following actomyosin ring disassembly is plotted. (**E**) Breakage near centromeres require condensin. Wild-type and *smc2-AID* cells possessing a 6+7 dicentric with no inserted tandem array proceeded through mitosis with or without 2mM IAA. Gel Red labelled PFGE shown in Supplemental Figure S2.

Figure 5: Preferential breakage at the pericentromeres of shorter dicentrics and at tandem Rap1 sites require condensin. (**A**) Condensin loss displaces breakage positions away from centromeres in shorter dicentrics. Dicentrics were generated through *CEN4* insertion in chromosome 6 right arm by homologous recombination (López et al., 2015). Wild-type and *smc2-AID* cells possessing a dicentric with a *CEN6-CEN4* distance of 100 kb or 45 kb proceeded through mitosis with or without 2mM IAA. Chromosomes separated by PFGE were probed with a fragment from chromosome 6 left arm. (**B**) Breakage at off-centre Rap1 sites requires condensin. Wild-type and *smc2-AID* cells possessing a 6+7 dicentric with 12 Rap1 binding sites inserted within chromosome 7 left arm at ~100 kb from *CEN7* proceeded through mitosis with or without 2mM IAA. (**C**) Breakage at centred Rap1 sites in the absence of condensin. Wild-type and *smc2-AID* cells possessing a 6+7 dicentric with 12 Rap1 binding sites inserted within chromosome 7 left arm at ~300 kb from *CEN7* proceeded through mitosis with or without 2mM IAA.

Left and right panels: two independent experiments. (**D**) Breakage at a telomere fusion located within the median region of a dicentric requires condensin. Dicentrics were generated through a fusion of chromosome 6 right end and chromosome 1 right end by homologous recombination. Left panel: wild-type and *smc2-AID* cells possessing a 6+1 dicentric with or without a head-to-head telomere fusion inserted at the junction between chromosomes 6 and 1 proceeded through mitosis with or without 2mM IAA. The inserted telomere fusion contains ~400 bp of telomere repeats. Right panel: independent duplicates of the *smc2-AID* context with telomere fusion. Gel Red labelled PFGE shown in Supplemental Figure S2.

Figure 6: Close spacing between tandem Rap1 sites is essential to establish a breakage hotspot. (**A**) Top panel: closely spaced Rap1 sites are alternatively separated by 1 and 6 bp. Bottom panel: in the interspaced array, the Rap1 sites are alternatively separated by 1 and 35 bp. A lacO site is present within this larger linker. (**B**) Preferential breakage at internal arrays of Rap1 binding sites with close spacing. Cells possess a 6+7 dicentric with 16 Rap1 binding sites in tandem (without or with lacO sites in between) inserted at the junction between chromosomes 6 and 7. Cells proceeded through mitosis with or without 2mM IPTG. High-affinity lacI is expressed from an integrated plasmid. Gel Red labelled PFGE shown in Supplemental Figure S2.

Figure 7: Models for dicentric dynamics, refolding and breakage in budding yeast. (**A**) Model for dicentric preferential breakage at pericentromeres. Condensin molecules are in orange, chromatin and centromeres in blue, SPBs and microtubules in brown, nuclear envelop and plasma membrane in black, cell wall and septum in grey. For simplicity, only one chromatid is drawn. The number and dynamics of the condensin molecules involved in dicentric refolding are unknown. (B) Model for dicentric breakage in the condensin-depleted cells. (C) Model for dicentrics preferential breakage at telomere fusions. (D) Model for the breakage of dicentrics with a telomere fusion in the condensin-depleted cells. The proposed scenarios are described in the discussion.

STAR Methods

Key Resources Table

Attached file.

Contact for Reagent and Resource Sharing

Further information and request for resources and reagents should be directed to and will be fulfilled by the Lead Contact, Stéphane Marcand (stephane.marcand@cea.fr).

Experimental Model and Subject Details

Strains and plasmids

The strains used in this study are listed in Supplemental Table S1. To fuse the chromosome 6 right end to the chromosome 7 left end at *ADH4*, cells were transformed with XhoI NotI cut plasmid sp1003 (deleting the distal end of 6R from coordinate 268139 (López et al., 2015)), sp625 (including the entire 6R subtelomere without TG_{1-3} repeats), sp626 (including the entire 6R subtelomere and 300 bp of TG_{1-3} repeats) and plasmids pCB22, pCB3, pCB23, pCB4 and pCB24 with 6 to 24 Rap1 sites respectively derived from sp1003. To fuse the chromosome 6 right end to the chromosome 1 right end at *IMD1*, cells were transformed with XhoI NotI cut plasmid pCB26 (including the entire 6R subtelomere without TG_{1-3} repeats) and sp630 (including the entire 6R subtelomere and a telomere-telomere fusion with approximately 450 bp of TG_{1-3} repeats). Integration is relatively inefficient but remarkably specific, probably due to the simultaneous double selection on galactose plates lacking leucine. The *CEN4-klLEU2* cassette was inserted in the chromosome 6 right arm through a PCR-mediated transformation as previously described (Longtine et al., 1998; López et al., 2015). The inserted Rap1 sites (underlined) are tandem arrays of the GATCC<u>TACACCCATACACCT</u><u>TACACCCAGACACCA</u> sequence (Grossi et al., 2001). The mutated Rap1 sites are tandem arrays of the GATCC<u>TACTCCCATACTCCT</u><u>TACTCCCAGACTCCA</u> sequence. The Rap1 sites (underlined) interspaced with lacO sites (bold) are a tandem array of the GATCC<u>TACACCCATACACCT</u><u>TACACCCAGACACCA</u>ATA**TGGAATTGTGAGCGGATAACAATT**TCA sequence.

The *smc2-AID* allele was created with plasmid pHyg-AID*-9myc::NAT or pHyg-AID*-9myc::HPH and osTIR1 inserted at URA3 after digestion of PNHK53 by StuI (Morawska and Ulrich, 2013). The *SPC42-yeGFP* and *MYO1-TTyeGFP* alleles were created with plasmids pYM26 and sp585, respectively, and the *SPC42-mCherry* allele was created with the plasmid pFA6-mCherry-HPHB-MX6. The TTyeGFP-Spo20$^{51-91}$ plasma membrane marker (Kuilman et al., 2015) is expressed from a plasmid integrated at the *URA3* locus.

The *GFP-lacI** and lacI-mCherry* alleles were integrated at the *URA3* locus with plasmids sp613 (*GFP-lacI***, *HIS3* promoter) and pAT165 (*lacI-mCherry, ADH1* promoter) (Dubarry et al., 2011). Both proteins are C-terminal truncated lacI ending at Leu^{350} and lacking the tetramerization sequence. The affinity of the lacI** allele is lowered by the insertion of three glycines replacing Gln^{60} in the hinge region, downstream of the DNA binding domain (Dubarry et al., 2011; Falcon and Matthews, 1999). In addition, the GFP tag in amino-terminal position can further decrease lacI** interaction with lacO. The mCherry tag of the high-affinity lacI is in carboxy-terminal position.

The *lacO* arrays (Lau et al., 2003) were integrated in chromosome 7 at coordinate 484500 (16.5 kb from *CEN7*) and coordinate 166500 (~330 kb from *CEN7)* with plasmids pAT381 (200 sites split in two blocks of 100 sites separated by ~800 bp; a gift from Angela Taddei, (Dubarry et al., 2011)), sp629 (100 sites) and sp628 (50 sites) as described in (Rohner et al., 2008). The *16 Rap1 sites-NAT* cassette was inserted through a PCR-mediated transformation in chromosome 7 at coordinates 413049 (at position 1/6) or coordinates 206707 (at position 1/2). Gene deletions were obtained through a PCR-mediated transformation as described in (Longtine et al., 1998). To generate a *myo1-Δ* strain, we first generated a diploid by crossing *bud4-* strain Lev752 and *BUD4+* strain 134-1a (López et al., 2015). One copy of *MYO1* was deleted. Viable *BUD4+ myo1-Δ* spores were backcrossed twice in the W303 background and restricted several times to select for normal growth, generating strains YTG84 and YTG87. Video-microscopy with the TTyeGFP-Spo20$^{51-91}$ plasma membrane marker confirmed the normal timing and efficiency of cytokinesis in these *myo1-Δ* strains.

Method Details

Cell cycle synchronization and protein degradation

Cells were arrested in G1 with 10^{-7} M α-factor (from a 10^{-3} M stock solution in ethanol) and released by two washes in rich medium. Cells were arrested in G2/M with 5

µg/mL nocodazole (from 1.5 mg/mL stock solution in DMSO) and released by 3 YPD 1 % DMSO washes. IAA (Sigma-Aldrich I2886) was added to a 2 mM final concentration (from 500 mM stock solution in ethanol). IPTG was added to a 2mM final concentration (from a 1 M stock solution in water) immediately after G1 or G2/M releases. The efficiency of the arrests and releases was checked by microscopy.

PFGE and Southern blot

Yeast DNA embedded in agarose plugs was prepared as follows. About $1\text{-}2.10^8$ cells were harvested, washed with 1 mL of 1% Triton, 250 mM EDTA, 10 mM Tris (pH 7.5) and frozen at -80°C. Pellets were resuspended in 120 µL of 50 mM EDTA, 10 mM Tris (pH 7.5), quickly warmed to 42°C and mixed with 200 µL of prewarmed 1% agarose LMP. The suspension was distributed into 80 µL wells placed on a cool surface. The plugs were extruded and incubated overnight at 37°C in 1 mL of 500 mM EDTA, 10 mM Tris (pH 7.5), 40 µg/mL of Zymolyase-100T (MP Biomedical 32093). The following day, plugs were incubated 6h at 53°C in 1 mL of 500 mM EDTA, 10 mM Tris (pH 8.0), 1% N-Laurylsarcosyl, 0.5 mg/mL Proteinase K (Invitrogen P/N 100005393). Plugs were washed for 30 minutes three times in 1 mL of 50 mM EDTA, 10 mM Tris (pH 7.5). Pulse-field electrophoresis was carried out in a 0,9% agarose gel in 0.5X TBE at 14°C with a CHEF DR III from Bio-Rad with a switch time ramping up from 60 to 120 seconds in 24 hours (to resolve the whole karyotype), with a switch time ramping up from 15 to 30 seconds in 24 hours (to resolve fragments from 20 to 400 kb; Figure 5A) or a switch time ramping up from 20 to 40 seconds in 24 hours (to resolve fragments from 50 to 600 kb; Figure 5D). Chromosomes were labelled with gel red and scanned (Supplemental Figures S2, S6 and S12) prior to blotting. The template for the Southern blot probe is a gel-purified PCR product of the *TUB2* gene amplified from yeast genomic DNA. Large chromosomes, including 6+7 dicentrics, can be fragmented during plug preparation, generating a smearing signal, a technical issue more frequent with G2/M arrested samples (for instance Figure 3B left panel *myo1-AID* cells in G2/M or Figure 5B right panel WT cells in G2/M).

Time-lapse microscopy

The higher resolution live-cell images of Figure 3A were acquired using an inverted Spinning Disk microscope (Nikon Eclipse Ti-E-ad and Yokogawa CSU-X1-A1) equipped

with a perfect focus system, a 100x APO TIRF/1.49NA immersion objective, a Prime 95B camera (Photometrics) and a Live-SR module (Roper). The system is piloted by MetaMorph software (Molecular Device). Cells were grown exponentially in synthetic medium and plated on synthetic medium 1% agarose pads before imaging at 30°C. GFP and mCherry images were acquired sequentially with an exposure of 50 msec using 491 nm (Cobolt Calypso, 100 mW) and 561 nm (Cobolt Jive, 150 mW) lasers, filters used were [BP 470/40, DM 495 nm, BP 520/35 (Nikon) and BP 560/40, DM 595 nm, BP 630/60 (Nikon) and dichroic triple BP 405/491/561 nm (Semrock)]. Further processing was done using ImageJ software (National Institute of Health).

Live-cell images of Figure 4 were acquired using a wide-field microscope based on an inverted microscope (Leica DMI-6000B) equipped with adaptive focus control to eliminate Z drift, a 100×/1.4 NA immersion objective with a Prior NanoScanZ Nanopositioning Piezo Z stage system, a CMOS camera (ORCA-Flash4.0, Hamamatsu), and a solid-state light source (SpectraX, Lumencore). The system is piloted by the MetaMorph software (Molecular Device). Cells were grown exponentially in synthetic medium, and 50 μL of the culture was loaded in microfluidic plates (Y04C plates, ONIX platform, CellASIC) equilibrated at 30°C for 2 hours. GFP and mCherry images were acquired sequentially for each Z section with an exposure time of 10 msec using solid-state 475- and 575-nm diodes and appropriate filters (GFP-mCherry filter, excitation: double BP, 450–490/550–590 nm, and dichroic double BP, 500–550/600–665 nm, Chroma Technology Corp.). For four-dimensional movies, 25 focal steps of 0.25 μm were taken every 2 minutes for 2 hours. Three-dimensional data sets were deconvolved using the AutoQuant blind deconvolution algorithm (Media Cybernetics, Inc.) with the point-spread function appropriate for our microscope at each emission wavelength. Further processing was done using ImageJ software (National Institutes of Health).

Hi-C libraries generation and sequencing

Aliquots of 1-3 x 10^9 cells in 150 ml YPD/synthetic medium were fixed in 3% formaldehyde (Sigma) for 20 min at room temperature and quenched with 25 ml glycine 2.5 M for 20 min at 4°C. Hi-C libraries were generated as described (Lazar-Stefanita et al., 2017), except that cells were disrupted using a Precellys apparatus (instead of being processed through zymolyase treatment) and that biotin-labeled fragments were selectively captured by Dynabeads Myone Streptavidin C1 (Invitrogen). The resulting

libraries were sequenced on a NextSeq500 Illumina apparatus. Contact maps were generated and normalized as described (Cournac et al., 2012).

Quantification and statistical analysis

Statistical analysis and data visualization were performed in PRISM (https://ritme.com/fr/logiciels/prism/).

Data and software availability

Raw data are available at http://dx.doi.org/10.17632/3hcgk2n27j.1

HiC whole genome and high-resolution maps are available at http://dx.doi.org/10.17632/2hdp26c722.1 and HiC sequencing data are available at https://www.ncbi.nlm.nih.gov/bioproject/PRJNA542278

Table S1. Yeast Strains Used in This Study. Related to STAR Methods.

Strains are from the W303-1a background (*ade2-1 trp1-1 ura3-1 leu2-3,112 his3-11,15 can1-100 RAD5*) except strain 234-1a from the RM11 background (*leu2-Δ ura3-Δ ho::loxP-KANr-loxP*).

References

Amaral, N., Vendrell, A., Funaya, C., Idrissi, F.-Z., Maier, M., Kumar, A., Neurohr, G., Colomina, N., Torres-Rosell, J., Geli, M.-I., et al. (2016). The Aurora-B-dependent NoCut checkpoint prevents damage of anaphase bridges after DNA replication stress. Nat. Cell Biol. *18*, 516–526.

Baxter, J., and Diffley, J.F.X. (2008). Topoisomerase II Inactivation Prevents the Completion of DNA Replication in Budding Yeast. Molecular Cell *30*, 790–802.

Benarroch-Popivker, D., Pisano, S., Mendez-Bermudez, A., Lototska, L., Kaur, P., Bauwens, S., Djerbi, N., Latrick, C.M., Fraisier, V., Pei, B., et al. (2016). TRF2-Mediated Control of Telomere DNA Topology as a Mechanism for Chromosome-End Protection. Molecular Cell *61*, 274–286.

Beyer, T., and Weinert, T. (2016). Ontogeny of Unstable Chromosomes Generated by Telomere Error in Budding Yeast. Plos Genet *12*, e1006345.

Bétermier, M., Bertrand, P., and Lopez, B.S. (2014). Is Non-Homologous End-Joining Really an Inherently Error-Prone Process? Plos Genet *10*, e1004086.

Bi, E., Maddox, P., Lew, D.J., Salmon, E.D., McMillan, J.N., Yeh, E., and Pringle, J.R. (1998). Involvement of an actomyosin contractile ring in Saccharomyces cerevisiae cytokinesis. J. Cell Biol. *142*, 1301–1312.

Bi, E., and Park, H.-O. (2012). Cell polarization and cytokinesis in budding yeast. Genetics *191*, 347–387.

Bloom, K.S. (2007). Beyond the code: the mechanical properties of DNA as they relate to mitosis. Chromosoma *117*, 103–110.

Brace, J.L., Doerfler, M.D., and Weiss, E.L. (2019). A cell separation checkpoint that enforces the proper order of late cytokinetic events. The Journal of Cell Biology *218*, 150–170.

Cabib, E., and Arroyo, J. (2013). How carbohydrates sculpt cells: chemical control of morphogenesis in the yeast cell wall. Nat. Rev. Microbiol. *11*, 648–655.

Candelli, T., Challal, D., Briand, J.-B., Boulay, J., Porrua, O., Colin, J., and Libri, D. (2018). High-resolution transcription maps reveal the widespread impact of roadblock termination in yeast. Embo J. *37*, e97490.

Challal, D., Barucco, M., Kubik, S., Feuerbach, F., Candelli, T., Geoffroy, H., Benaksas, C., Shore, D., and Libri, D. (2018). General Regulatory Factors Control the Fidelity of Transcription by Restricting Non-coding and Ectopic Initiation. Mol. Cell *72*, 955–969.e957.

Cheng, T.M.K., Heeger, S., Chaleil, R.A.G., Matthews, N., Stewart, A., Wright, J., Lim, C., Bates, P.A., and Uhlmann, F. (2015). A simple biophysical model emulates budding yeast chromosome condensation. eLife *4*, e05565.

Cournac, A., Marie-Nelly, H., Marbouty, M., Koszul, R., and Mozziconacci, J. (2012). Normalization of a chromosomal contact map. BMC Genomics *13*, 436.

Cuylen, S., Metz, J., Hruby, A., and Haering, C.H. (2013). Entrapment of Chromosomes by Condensin Rings Prevents Their Breakage during Cytokinesis. Developmental Cell *27*, 469–478.

Diebold-Durand, M.-L., Lee, H., Ruiz Avila, L.B., Noh, H., Shin, H.-C., Im, H., Bock, F.P., Bürmann, F., Durand, A., Basfeld, A., et al. (2017). Structure of Full-Length SMC and Rearrangements Required for Chromosome Organization. Molecular Cell *67*, 334–347.e335.

Dubarry, M., Loiodice, I., Chen, C.L., Thermes, C., and Taddei, A. (2011). Tight protein-DNA interactions favor gene silencing. Genes & Development *25*, 1365–1370.

Ebrahimi, H., and Donaldson, A.D. (2008). Release of yeast telomeres from the nuclear periphery is triggered by replication and maintained by suppression of Ku-mediated anchoring. Genes & Development *22*, 3363–3374.

Ebrahimi, H., Robertson, E.D., Taddei, A., Gasser, S.M., Donaldson, A.D., and Hiraga, S.-I. (2010). Early initiation of a replication origin tethered at the nuclear periphery. Journal of Cell Science *123*, 1015–1019.

Eeftens, J.M., Bisht, S., Kerssemakers, J., Kschonsak, M., Haering, C.H., and Dekker, C. (2017). Real-time detection of condensin-driven DNA compaction reveals a multistep binding mechanism. Embo J. *36*, 3448–3457.

Falcon, C.M., and Matthews, K.S. (1999). Glycine insertion in the hinge region of lactose repressor protein alters DNA binding. J. Biol. Chem. *274*, 30849–30857.

Ganji, M., Shaltiel, I.A., Bisht, S., Kim, E., Kalichava, A., Haering, C.H., and Dekker, C. (2018). Real-time imaging of DNA loop extrusion by condensin. Science *360*, 102–105.

Gibcus, J.H., Samejima, K., Goloborodko, A., Samejima, I., Naumova, N., Nuebler, J., Kanemaki, M.T., Xie, L., Paulson, J.R., Earnshaw, W.C., et al. (2018). A pathway for mitotic chromosome formation. Science *359*.

Goto, G.H., Zencir, S., Hirano, Y., Ogi, H., Ivessa, A., and Sugimoto, K. (2015). Binding of Multiple Rap1 Proteins Stimulates Chromosome Breakage Induction during DNA Replication. Plos Genet *11*, e1005283.

Grossi, S., Bianchi, A., Damay, P., and Shore, D. (2001). Telomere formation by rap1p binding site arrays reveals end-specific length regulation requirements and active telomeric recombination. Mol. Cell. Biol. *21*, 8117–8128.

Hill, A., and Bloom, K. (1989). Acquisition and processing of a conditional dicentric chromosome in Saccharomyces cerevisiae. Mol. Cell. Biol. *9*, 1368–1370.

Hirano, T., Funahashi, S., Uemura, T., and Yanagida, M. (1986). Isolation and characterization of Schizosaccharomyces pombe cutmutants that block nuclear division but not cytokinesis. Embo J *5*, 2973–2979.

Hirano, T. (2017). Capturing condensin in chromosomes. Nat. Genet. *49*, 1419–1420.

Hocquet, C., Robellet, X., Modolo, L., Sun, X.-M., Burny, C., Cuylen-Haering, S., Toselli, E., Clauder-Münster, S., Steinmetz, L., Haering, C.H., et al. (2018). Condensin controls cellular RNA levels through the accurate segregation of chromosomes instead of directly regulating transcription. eLife *7*.

Hong, Y., Sonneville, R., Wang, B., Scheidt, V., Meier, B., Woglar, A., Demetriou, S., Labib, K., Jantsch, V., and Gartner, A. (2018a). LEM-3 is a midbody-tethered DNA nuclease that resolves chromatin bridges during late mitosis. Nature Communications *9*, 728.

Hong, Y., Velkova, M., Silva, N., Jagut, M., Scheidt, V., Labib, K., Jantsch, V., and Gartner, A. (2018b). The conserved LEM-3/Ankle1 nuclease is involved in the combinatorial regulation of meiotic recombination repair and chromosome segregation in Caenorhabditis elegans. Plos Genet *14*, e1007453.

Hou, H., and Cooper, J.P. (2018). Stretching, scrambling, piercing and entangling: Challenges for telomeres in mitotic and meiotic chromosome segregation. Differentiation *100*, 12–20.

Kaddour, A., Colicchio, B., Buron, D., Maalouf, El, E., Laplagne, E., Borie, C., Ricoul, M., Lenain, A., Hempel, W.M., Morat, L., et al. (2017). Transmission of Induced Chromosomal Aberrations through Successive Mitotic Divisions in Human Lymphocytes after In Vitro and In Vivo Radiation. Sci Rep *7*, 3291.

Knight, B., Kubik, S., Ghosh, B., Bruzzone, M.J., Geertz, M., Martin, V., Dénervaud, N., Jacquet, P., Ozkan, B., Rougemont, J., et al. (2014). Two distinct promoter architectures centered on dynamic nucleosomes control ribosomal protein gene transcription. Genes Dev. *28*, 1695–1709.

Koc, K.N., Singh, S.P., Stodola, J.L., Burgers, P.M., and Galletto, R. (2016). Pif1 removes a Rap1-dependent barrier to the strand displacement activity of DNA polymerase δ. Nucleic Acids Research *44*, 3811–3819.

Kschonsak, M., Merkel, F., Bisht, S., Metz, J., Rybin, V., Hassler, M., and Haering, C.H. (2017). Structural Basis for a Safety-Belt Mechanism That Anchors Condensin to Chromosomes. Cell *171*, 588–600.e24.

Kubik, S., O'Duibhir, E., de Jonge, W.J., Mattarocci, S., Albert, B., Falcone, J.-L., Bruzzone, M.J., Holstege, F.C.P., and Shore, D. (2018). Sequence-Directed Action of RSC Remodeler and General Regulatory Factors Modulates +1 Nucleosome Position to Facilitate Transcription. Mol. Cell *71*, 89–102.e5.

Kuilman, T., Maiolica, A., Godfrey, M., Scheidel, N., Aebersold, R., and Uhlmann, F. (2015). Identification of Cdk targets that control cytokinesis. Embo J *34*, 81–96.

Lau, I.F., Filipe, S.R., Søballe, B., Økstad, O.-A., Barre, F.-X., and Sherratt, D.J. (2003). Spatial and temporal organization of replicating Escherichia coli chromosomes. Molecular Microbiology *49*, 731–743.

Lavoie, B.D., Hogan, E., and Koshland, D. (2004). In vivo requirements for rDNA chromosome condensation reveal two cell-cycle-regulated pathways for mitotic chromosome folding. Genes & Development *18*, 76–87.

Lazar-Stefanita, L., Scolari, V.F., Mercy, G., Muller, H., Guérin, T.M., Thierry, A., Mozziconacci, J., and Koszul, R. (2017). Cohesins and condensins orchestrate the 4D dynamics of yeast chromosomes during the cell cycle. Embo J. *36*, 2684–2697.

Le Bihan, Y.-V., Matot, B., Pietrement, O., Giraud-Panis, M.-J., Gasparini, S., Le Cam, E., Gilson, E., Sclavi, B., Miron, S., and Le Du, M.-H. (2013). Effect of Rap1 binding on DNA distortion and potassium permanganate hypersensitivity. Acta Crystallogr. D Biol. Crystallogr. *69*, 409–419.

Lescasse, R., Pobiega, S., Callebaut, I., and Marcand, S.E.P. (2013). End-joining inhibition at telomeres requires the translocase and polySUMO-dependent ubiquitin ligase Uls1. Embo J. *32*, 805-815.

Lickwar, C.R., Mueller, F., Hanlon, S.E., McNally, J.G., and Lieb, J.D. (2012). Genome-wide protein-DNA binding dynamics suggest a molecular clutch for transcription factor function. Nature *484*, 251–255.

Longtine, M.S., McKenzie, A., Demarini, D.J., Shah, N.G., Wach, A., Brachat, A., Philippsen, P., and Pringle, J.R. (1998). Additional modules for versatile and economical PCR-based gene deletion and modification in Saccharomyces cerevisiae. Yeast *14*, 953–961.

López, V., Barinova, N., Onishi, M., Pobiega, S., Pringle, J.R., Dubrana, K., and Marcand, S. (2015). Cytokinesis breaks dicentric chromosomes preferentially at pericentromeric regions and telomere fusions. Genes & Development *29*, 322–336.

Maciejowski, J., and de Lange, T. (2017). Telomeres in cancer: tumour suppression and genome instability. Nat. Rev. Mol. Cell Biol. *18*, 175–186.

Maciejowski, J., Li, Y., Bosco, N., Campbell, P.J., and de Lange, T. (2015). Chromothripsis and Kataegis Induced by Telomere Crisis. Cell *163*, 1641–1654.

Marko, J.F., De Los Rios, P., Barducci, A., and Gruber, S. (2018). DNA-segment-capture model for loop extrusion by structural maintenance of chromosome (SMC) protein complexes. bioRxiv 325373.

Matot, B., Le Bihan, Y.V., Lescasse, R., Perez, J., Miron, S., David, G., Castaing, B., Weber, P., Raynal, B., Zinn-Justin, S., et al. (2012). The orientation of the C-terminal domain of the Saccharomyces cerevisiae Rap1 protein is determined by its binding to DNA. Nucleic Acids Research *40*, 3197–3207.

McClintock, B. (1941). The Stability of Broken Ends of Chromosomes in Zea Mays. Genetics *26*, 234–282.

Miller, M.P., Asbury, C.L., and Biggins, S. (2016). A TOG Protein Confers Tension Sensitivity to Kinetochore-Microtubule Attachments. Cell *165*, 1428–1439.

Mohebi, S., Mizuno, K., Watson, A., Carr, A.M., and Murray, J.M. (2015). Checkpoints are blind to replication restart and recombination intermediates that result in gross chromosomal rearrangements. Nature Communications *6*, 6357.

Morawska, M., and Ulrich, H.D. (2013). An expanded tool kit for the auxin-inducible degron system in budding yeast. Yeast *30*, 341–351.

Muller, H.J., and Altenburg, E. (1930). The Frequency of Translocations Produced by X-Rays in Drosophila. Genetics *15*, 283–311.

Müller, C.A., Hawkins, M., Retkute, R., Malla, S., Wilson, R., Blythe, M.J., Nakato, R., Komata, M., Shirahige, K., de Moura, A.P.S., et al. (2014). The dynamics of genome replication using deep sequencing. Nucleic Acids Res. *42*, e3.

Müller, S., and Almouzni, G. (2017). Chromatin dynamics during the cell cycle at centromeres. Nature Publishing Group *18*, 192–208.

M'kacher, R., Maalouf, E.E.L., Ricoul, M., Heidingsfelder, L., Laplagne, E., Cuceu, C., Hempel, W.M., Colicchio, B., Dieterlen, A., and Sabatier, L. (2014). New tool for biological dosimetry: Reevaluation and automation of the gold standard method following telomere and centromere staining. Mutat. Res. *770*, 45–53.

Nasmyth, K. (2017). How are DNAs woven into chromosomes? Science *358*, 589–590.

Onishi, M., Ko, N., Nishihama, R., and Pringle, J.R. (2013). Distinct roles of Rho1, Cdc42, and Cyk3 in septum formation and abscission during yeast cytokinesis. J. Cell Biol. *202*, 311–329.

Pampalona, J., Roscioli, E., Silkworth, W.T., Bowden, B., Genescà, A., Tusell, L., and Cimini, D. (2016). Chromosome Bridges Maintain Kinetochore-Microtubule Attachment throughout Mitosis and Rarely Break during Anaphase. PLoS ONE *11*, e0147420.

Pobiega, S., and Marcand, S. (2010). Dicentric breakage at telomere fusions. Genes & Development *24*, 720–733.

Proctor, S.A., Minc, N., Boudaoud, A., and Chang, F. (2012). Contributions of Turgor Pressure, the Contractile Ring, and Septum Assembly to Forces in Cytokinesis in Fission Yeast. Current Biology *22*, 1601–1608.

Quevedo, O., García-Luis, J., Matos-Perdomo, E., Aragón, L., and Machín, F. (2012). Nondisjunction of a Single Chromosome Leads to Breakage and Activation of DNA Damage Checkpoint in G2. Plos Genet *8*, e1002509.

Rancati, G., Pavelka, N., Fleharty, B., Noll, A., Trimble, R., Walton, K., Perera, A., Staehling-Hampton, K., Seidel, C.W., and Li, R. (2008). Aneuploidy underlies rapid adaptive evolution of yeast cells deprived of a conserved cytokinesis motor. Cell *135*, 879–893.

Reis, C.C., Batista, S., and Ferreira, M.G. (2012). The fission yeast MRN complex tethers dysfunctional telomeres for NHEJ repair. Embo J. *31*, 4576–4586.

Renshaw, M.J., Ward, J.J., Kanemaki, M., Natsume, K., Nédélec, F.J., and Tanaka, T.U. (2010). Condensins Promote Chromosome Recoiling during Early Anaphase to Complete Sister Chromatid Separation. Developmental Cell *19*, 232–244.

Reyes, C., Serrurier, C., Gauthier, T., Gachet, Y., and Tournier, S. (2015). Aurora B prevents chromosome arm separation defects by promoting telomere dispersion and disjunction. The Journal of Cell Biology *208*, 713–727.

Robellet, X., Thattikota, Y., Wang, F., Wee, T.-L., Pascariu, M., Shankar, S., Bonneil, É., Brown, C.M., and D'Amours, D. (2015). A high-sensitivity phospho-switch triggered by Cdk1 governs chromosome morphogenesis during cell division. Genes Dev. *29*, 426–439.

Rohner, S., Gasser, S.M., and Meister, P. (2008). Modules for cloning-free chromatin tagging in Saccharomyces cerevisae. Yeast *25*, 235–239.

Shintomi, K., Inoue, F., Watanabe, H., Ohsumi, K., Ohsugi, M., and Hirano, T. (2017). Mitotic chromosome assembly despite nucleosome depletion in Xenopus egg extracts. Science *356*, 1284–1287.

Song, W., Gawel, M., Dominska, M., Greenwell, P.W., Hazkani-Covo, E., Bloom, K., and Petes, T.D. (2013). Nonrandom distribution of interhomolog recombination events induced by breakage of a dicentric chromosome in Saccharomyces cerevisiae. Genetics *194*, 69–80.

Sun, M., Biggs, R., Hornick, J., and Marko, J.F. (2018). Condensin controls mitotic chromosome stiffness and stability without forming a structurally contiguous scaffold. Chromosome Res. *26*, 277–295.

Suto, Y. (2016). Review of Cytogenetic analysis of restoration workers for Fukushima Daiichi nuclear power station accident. Radiat Prot Dosimetry *171*, 61–63.

Swygert, S.G., Kim, S., Wu, X., Fu, T., Hsieh, T.-H., Rando, O.J., Eisenman, R.N., Shendure, J., McKnight, J.N., and Tsukiyama, T. (2018). Condensin-Dependent Chromatin Compaction Represses Transcription Globally during Quiescence. Molecular Cell.

Tanaka, K., Mukae, N., Dewar, H., van Breugel, M., James, E.K., Prescott, A.R., Antony, C., and Tanaka, T.U. (2005). Molecular mechanisms of kinetochore capture by spindle microtubules. Nature *434*, 987–994.

Thadani, R., Kamenz, J., Heeger, S., Muñoz, S., and Uhlmann, F. (2018). Cell-Cycle Regulation of Dynamic Chromosome Association of the Condensin Complex. Cell Rep *23*, 2308–2317.

Thattikota, Y., Tollis, S., Palou, R., Vinet, J., Tyers, M., and D'Amours, D. (2018). Cdc48/VCP Promotes Chromosome Morphogenesis by Releasing Condensin from Self-Entrapment in Chromatin. Molecular Cell *69*, 664–676.e665.

Thrower, D.A., and Bloom, K. (2001). Dicentric chromosome stretching during anaphase reveals roles of Sir2/Ku in chromatin compaction in budding yeast. Molecular Biology of the Cell *12*, 2800–2812.

van Steensel, B., Smogorzewska, A., and de Lange, T. (1998). TRF2 protects human telomeres from end-to-end fusions. Cell *92*, 401–413.
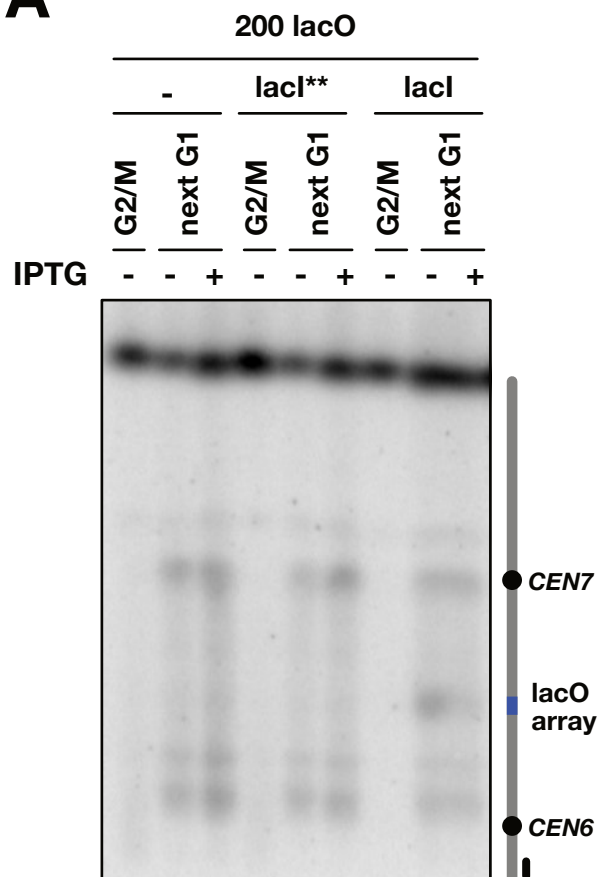
Voth, W.P., Olsen, A.E., Sbia, M., Freedman, K.H., and Stillman, D.J. (2005). ACE2, CBK1, and BUD4 in budding and cell separation. Eukaryotic Cell *4*, 1018–1028.

Weiss, E.L. (2012). Mitotic Exit and Separation of Mother and Daughter Cells. Genetics *192*, 1165–1202.
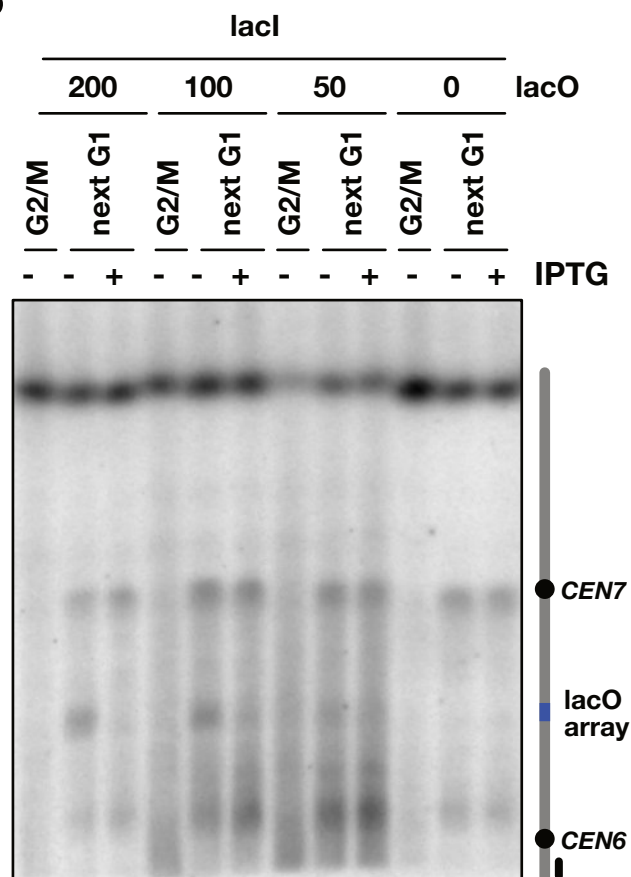
Wellinger, R.J., and Zakian, V.A. (2012). Everything you ever wanted to know about Saccharomyces cerevisiae telomeres: beginning to end. Genetics *191*, 1073–1105.

Williams, T.L., Levy, D.L., Maki-Yonekura, S., Yonekura, K., and Blackburn, E.H. (2010). Characterization of the yeast telomere nucleoprotein core: Rap1 binds independently to each recognition site. J. Biol. Chem. *285*, 35814–35824.

A

GFP-Spo20^51-91   H2A-mCherry

time in minutes

B

-                           24 Rap1 sites

WT   myo1-AID   adapted myo1-Δ   WT   myo1-AID   adapted myo1-Δ

G2/M | next G1   G2/M | next G1   G2/M | next G1   G2/M | next G1   G2/M | next G1   G2/M | next G1

- - +   - - +   - - +   - - +   - - +   - - +   IAA

CEN7

Rap1 sites

CEN6

C

0   24 Rap1 sites

WT   ace2-Δ   WT   ace2-Δ

G2/M | next G1   G2/M | next G1   G2/M | next G1   G2/M | next G1

A

GFP-Spo20⁵¹⁻⁹¹   Spc42-mCherry

time in minutes

C

Myo1-GFP   Spc42-mCherry
GFP-lacI**/lacO at *CEN7*

time in minutes

B

D

E

A

16 Rap1 sites

Rap1

Rap1   Rap1   Rap1   Rap1

TACACCCATACACCT TACACCCAGACACC AGATCC TACACCCATACACCT TACACCCAGACACC

6 bp

16 Rap1 sites interspaced with lacO sites

Rap1   Rap1   lacO   8 bp   Rap1   Rap1

TACACCCATACACCT TACACCCAGACACC ATA TGGAATTGTGAGCGGATAACAATT TCAGATCC TACACCCATACACCT TACACCCAGACACC

35 bp

B

| | 16 Rap1 sites | 16 Rap1 sites interspaced with lacO sites | |
| | - | - | lacI |

CEN7

Rap1 / lacO array

CEN6

Condensin

Rap1

Septa